Journal of Physics and Chemistry of Solids 110 (2017) 152–160

Contents lists available at ScienceDirect

Journal of Physics and Chemistry of Solids

journal homepage: www.elsevier.com/locate/jpcs

Effects of the addition of Co, Ni or Cr on the decolorization properties of Fe-Si-B amorphous alloys

Changqin Zhang [a,*], Zhengwang Zhu [b], Haifeng Zhang [b]

[a] School of Materials Science and Engineering, Shandong Jianzhu University, Jinan 250101, China
[b] Shenyang National Laboratory for Materials Science, Chinese Academy of Sciences, Shenyang 110016, China

ARTICLE INFO

Keywords:
Fe-based amorphous alloys
Surface structures
Decolorization properties
Azo dyes

ABSTRACT

Fe-based amorphous alloys show great potential in degrading azo dyes and other organic pollutants, and are widely investigated as a kind of environmental-friendly materials for wastewater remediation. In this paper, the effects of Co, Ni or Cr addition on the decolorization properties of Fe-Si-B amorphous alloys were studied, and the mechanism of their different effects was analyzed. Co addition could lower the activation energy of Fe-Si-B amorphous alloys in decolorizing azo dyes, and had no weakening effect on the decolorization capability of Fe-Si-B amorphous alloys. Ni addition led to partial crystallization of Fe-Si-B amorphous alloys, and the decolorization mechanism at low temperatures changed from chemical degradation to physical adsorption. Cr addition could enhance the corrosion resistance of Fe-Si-B amorphous alloys, but the amorphous alloys completely lost the decolorization capability no matter at lower or higher temperatures. The results of X-ray photoelectron spectroscopy (XPS) and scanning electron microscopy (SEM) indicated that the addition of Co, Ni or Cr could generate different surface structures that had significant influences on the decolorization process. Our work demonstrated that the effiecient decolorization of azo dyes by Fe-based alloys could be realized only when amorphous nature and incompact surface structure were simultaneously achieved for the alloys.

1. Introduction

Since amorphous alloys were firstly reported in decolorizing azo dyes [1], a few studies have been carried out on the degradation of azo dyes in aqueous solution by various amorphous alloys such as Fe-based alloys [2–12], Mg-based alloys [13–15], Co-based alloys [16] and Al-based alloys [17], due to their advanced catalytic capability for wastewater remediation. These amorphous alloys may exist in ultrathin ribbon state or ultrafine powder state to achieve a large surface specific area, and some porous structures are also introduced to obtain a high surface utilization percentage of effective decolorizing elements. Each of these amorphous alloys can achieve ultrafast dye degradation under proper conditions.

The efficient decolorization of azo dyes is generally attributed to the amorphous nature or the metastable thermodynamic feature and the incompact surface structures of amorphous alloys [2,3,9,10]. The amorphous nature or the metastable thermodynamic feature can endow the alloys with a higher energy level compared with their crystalline counterparts, which lowers the activation energy of the decolorization reaction and accelerates the decolorization rate. On the other hand, the incompact surface structures are necessary for the efficient decolorization, because the cleavage of —N═N– bonds in dye molecules involves electron transfer from zero-valent iron. If the surface layer of the alloys is too compact to hinder the dye solution from contacting with the inner zero-valent metal, then the reaction would be terminated once the superficial metallic atoms are consumed. In our previous work [2,5], as well as some other literature [3,13,16], amorphous nature of the alloys was emphasized, and the decolorization properties of amorphous alloys and their crystalline counterparts were extensively compared. It was considered that the higher energy level of the metastable thermodynamic state could provide more active sites for the decolorization reaction, which played a critical role in enhancing the decolorization efficiency. Quite recently, Tang et al. investigated the reaction kinetics, pathway and mechanism behind the high reactivity of Fe-B and Fe-Si-B amorphous alloys [9,10]. They considered that the addition of metalloid elements (B or Si and B) was conducive to the formation of an incompact and easily detached layer on the alloy surface, which could ensure the continuous contact of dye solution with the inner zero-valent iron. As a result, the crystalline counterparts of Fe-B and Fe-Si-B amorphous alloys showed significantly higher decolorization rate constant than zero-valent iron

* Corresponding author.
E-mail address: zhangcq@alum.imr.ac.cn (C. Zhang).

http://dx.doi.org/10.1016/j.jpcs.2017.06.010
Received 22 April 2017; Received in revised form 24 May 2017; Accepted 7 June 2017
Available online 8 June 2017

powder that had a native compact oxide layer.

Among amorphous alloys for azo dye decolorization, Fe-based amorphous alloys are easy to be recycled and have an acceptable level of decolorization efficiency decay owing to their superior soft magnetic property and chemical stability, so that their decolorization properties and related mechanism investigation have attracted much attention from this field [2–12]. As is well known, the addition of alloying elements can not only affect the glass-forming ability of amorphous alloys, but also have significant influences on their surface structures. In view of this, three alloying elements, Co, Ni and Cr, were respectively added into the glass-forming alloy composition $Fe_{78}Si_8B_{14}$ to produce three Fe-based alloys with nominal compositions of $Fe_{68}Co_{10}Si_8B_{14}$, $Fe_{68}Ni_{10}Si_8B_{14}$ and $Fe_{68}Cr_{10}Si_8B_{14}$. Their structures were characterized, and the decolorization properties were examined at different temperatures. Finally, the mechanism for their different decolorization properties was discussed and some insights were provided for understanding the roles of the amorphous nature and surface structure in decolorizing azo dyes.

2. Material and methods

Alloy ingots with nominal compositions of $Fe_{78}Si_8B_{14}$, $Fe_{68}Co_{10}Si_8B_{14}$, $Fe_{68}Ni_{10}Si_8B_{14}$ and $Fe_{68}Cr_{10}Si_8B_{14}$ were produced respectively by arc melting under Ti-gettered Ar atmosphere. Various ribbons of about 2 mm in width and 30–40 μm in thickness were then prepared by the single roller melt spinning method under an argon atmosphere. The ribbons were cut into small pieces with an area of about $2 \times 10\ mm^2$ for decolorization reaction. Acid orange II powder (wt.% $\geq$ 99.9%) was dissolved in distilled water to obtain an aqueous solution. Afterwards, the decolorization effects of different ribbons on 180 mL dye solution of 100 mg/L in a beaker were investigated respectively. The beaker was placed in a constant temperature water–bath trough at scheduled temperatures, and mechanical stirring of 200 r/min was applied in the beaker during the reaction process. In all experiments, the nominal surface area of ribbons was 15000 mm^2 to ensure a constant surface area concentration of $8.33 \times 10^{-2}\ m^2/L$. About 5 mL solution was taken from the beaker at intervals, and subjected to UV–vis spectrum scanning from 200 to 600 nm using a UV–visible spectrophotometer (Model V-550 JAS. CO., USA) after filtration through a 0.45 μm membranous filter. The dye concentration of the solution can be calculated by virtue of the method in **Ref.** [4].

The structures of the ribbons before decolorization reaction were examined by X-ray diffraction (XRD) with Cu-K_α radiation (D/max-2500PC, Rigaku Co., Japan). The surface morphologies before and after decolorization reaction were observed by a Cambridge S360 conventional scanning electron microscopy (SEM). X-ray photoelectron spectroscopy (XPS) was performed on a Thermo Scientific ESCALAB 250Xi instrument with Al- K_α radiation.

3. Results

3.1. Sample characterization results

Fig. 1 shows the XRD patterns of $Fe_{78}Si_8B_{14}$ and $Fe_{68}M_{10}Si_8B_{14}$ (M = Co, Ni, Cr). As can be seen, the XRD patterns of $Fe_{68}Co_{10}Si_8B_{14}$ and $Fe_{68}Cr_{10}Si_8B_{14}$ both show a single diffuse peak without any diffraction peaks, which means that the amorphous structure of $Fe_{78}Si_8B_{14}$ alloy is well retained after Co or Cr addition. In contrast, after Ni addtion, there appears a diffraction peak at $2\theta = 64.9°$ corresponding to α-Fe (200) in the XRD pattern, indicating that partial crystallization has occurred in the $Fe_{68}Ni_{10}Si_8B_{14}$ alloy ribbons.

Table 1 gives the surface element compositions of $Fe_{78}Si_8B_{14}$ and $Fe_{68}M_{10}Si_8B_{14}$ (M = Co, Ni, Cr) by XPS depth analysis. It can be seen that the content of oxygen element, including the adsorbed oxygen and combined oxygen, is very high for all ribbons in the outermost surface layer, which is up to 60%–70%. After Ar^+ sputtering for 10 s, the adsorbed oxygen on the surface is basically eliminated, and the oxygen

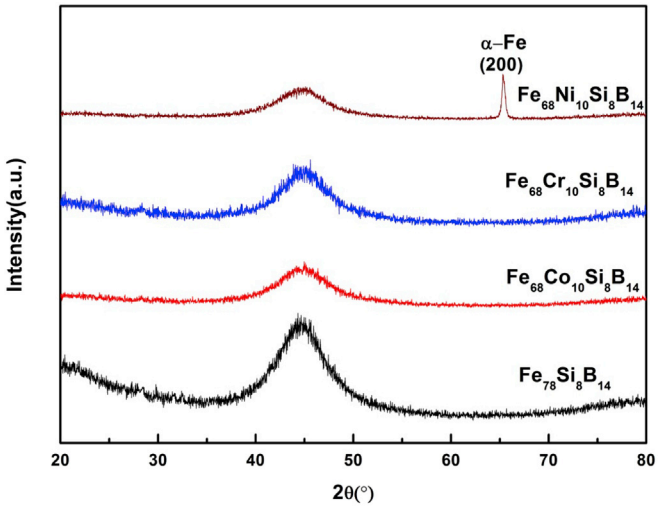

Fig. 1. XRD patterns of $Fe_{78}Si_8B_{14}$ and $Fe_{68}M_{10}Si_8B_{14}$ (M = Co, Ni, Cr).

Table 1
Surface element compositions of $Fe_{78}Si_8B_{14}$ and $Fe_{68}M_{10}Si_8B_{14}$ (M = Co, Ni, Cr) by XPS depth analysis.

Sputtering time(s)	Relative element content (at. %)			
	$Fe_{78}Si_8B_{14}$			
	Fe	Si	B	O
0	11.6	14.2	7.5	66.7
10	43.1	3.9	9.8	43.2
20	77.8	5.1	13.3	3.8

Sputtering time(s)	Relative element content (at. %)				
	$Fe_{68}Co_{10}Si_8B_{14}$				
	Fe	Co	Si	B	O
0	11.9	0.8	10.1	8.8	68.4
10	28.8	1.9	10.9	11.2	47.3
20	65.9	7.7	7.5	14.2	4.7
	$Fe_{68}Ni_{10}Si_8B_{14}$				
	Fe	Ni	Si	B	O
0	11.2	0.9	7.0	8.6	72.3
10	34.2	3.1	9.2	11.9	41.6
20	65.9	9.7	6.4	14.0	4.0
	$Fe_{68}Cr_{10}Si_8B_{14}$				
	Fe	Cr	Si	B	O
0	19.2	3.0	6.3	7.7	63.8
10	27.6	6.3	8.4	9.7	48.0
20	43.9	8.3	8.3	10.7	28.9
40	68.1	6.3	7.1	16.1	2.4

element exists only in the combined state to form the oxide layer with other elements. For $Fe_{78}Si_8B_{14}$, $Fe_{68}Ni_{10}Si_8B_{14}$ and $Fe_{68}Ni_{10}Si_8B_{14}$ ribbons, the oxygen content in the surface layer decreases to 3.8%, 4.7% and 4.0% respectively after Ar^+ sputtering for 20 s, indicating that the oxide layer has been etched away from the ribbons. Considering the instrument parameter settings of the photoelectron spectrometer (the sputtering rate for Ta_2O_5 was set as 0.4 nm/s), the thickness of the oxidation layer on the surface of the as-spun ribbons is about several nanometers. By contrast, for $Fe_{68}Cr_{10}Si_8B_{14}$ ribbons, the oxygen content is still as high as 28.9% after Ar^+ sputtering for 20 s. That is to say, there are still quite a few oxides at the depth of several nanometers underneath the surface of $Fe_{68}Cr_{10}Si_8B_{14}$ ribbons.

After the atomic percentage of oxygen in the surface layer of the ribbons is deducted (see Table 2), it can be found that in the outermost